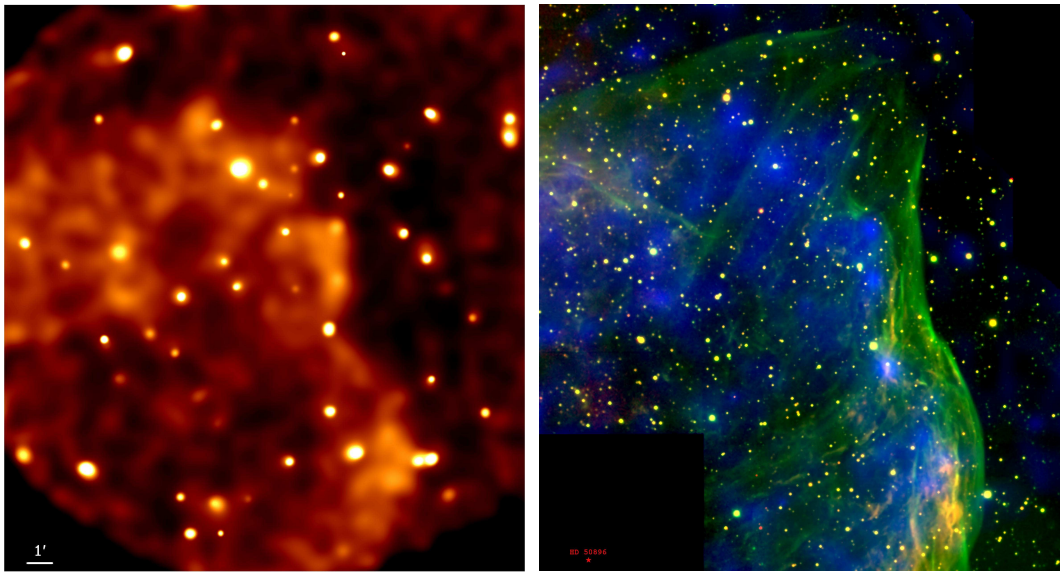

XMM-Newton: Guest Observer Facility, Guest Observer Funding, US Instrument Teams, and Education and Public Outreach

Prepared by: R. Mushotzky, NASA/GSFC, US Mission Scientist,
the US *XMM-Newton* Users Group (R. Griffiths, Chair),
and staff of the US Instrument Teams and *XMM-Newton* GOF

Summary

On behalf of the United States (US) *Newton X-ray Multi-Mirror Observatory* (*XMM-Newton*) users community, the US Instrument Teams, the National Aeronautics and Space Administration (NASA) Goddard Space Flight Center (GSFC) Guest Observer Facility (GOF), and the NASA *XMM-Newton* Education and Public Outreach (E/PO) program, we request funding for the continued support of US participation in the European Space Agency (ESA) *XMM-Newton* mission. The reasons for doing so are compelling: the exceptional scientific return, the complementarity of *XMM-Newton* and *Chandra* observations, and the particularly low cost to NASA for enabling access by US astronomers to Great-Observatory class observations. The response by the US astronomical community to the three Announcements of Opportunities (AOs) for submitting *XMM-Newton* Guest Observer (GO) proposals was extensive, with roughly one third of all the proposals having US Principle Investigators (PIs). The success rate for US PIs has also been quite good with more than one-third of the accepted proposals being awarded to US scientists ($\sim 40\%$ in AO-3). Of the remaining accepted proposals, roughly half have US Co-Investigators (Co-Is), thus two-thirds of all GO projects have US participation. ESA has allocated resources to support European *XMM-Newton* users, but has looked to the US GOF to provide support to the large US community. *XMM-Newton* observations provide excellent data for the study of a wide variety of astrophysical phenomena primarily supporting the NASA Structure and Evolution of the Universe (SEU) theme. Below we present the scientific return of *XMM-Newton*, the activities of the US instrument teams, the services provided by the GOF, *XMM-Newton* E/PO activities, and the proposed budget.

Mission Overview

XMM-Newton is the second cornerstone of the ESA *Horizon 2000* program. It was launched on 1999 December 10, and remains in full operation and in excellent health. ESA mission support is confirmed through 2008, with a high probability of future extensions. As of 2004 February 29, over 3460 targets had been observed. All science data are made public after the expiration of a proprietary period, one year for GO data. The *XMM-Newton* archive had 2412 observations publicly available as of 2004 February 29. As of March 2004, there have been 369 refereed papers published based on *XMM-Newton* data with another 71 "in press" (see Figure 1 and the publication list: http://xmm.gsfc.nasa.gov/docs/xmm/xmmhp_bibliography.html). In the first quarter of 2004, *XMM-Newton* produced more refereed publications than *Chandra* for the first time.

XMM-Newton excels in providing high throughput X-ray imaging and spectroscopy for the widest variety of astrophysical sources, from comets and planets to quasars and clusters of galaxies. The results thus far have demonstrated the importance of the mission in nearly all areas of astrophysics. The exploitation of the enormous archive of serendipitous sources is just beginning, and will continue for many years to come. The combination of *Chandra*, *XMM-Newton*, and soon *Astro-E2*, gives the world community the best possible combination of high angular resolution, high throughput, and high spectral resolution in the 0.2–12 keV band. Given the extensive participation by US GOs and their high rate of success in the AO process and the high proposal pressure (roughly seven times oversubscribed), *XMM-Newton* is clearly perceived as one of the world's pre-eminent astronomical observatories. Without US community access to *XMM-Newton*, US scientists will be placed at a severe disadvantage in many areas of astrophysical research.

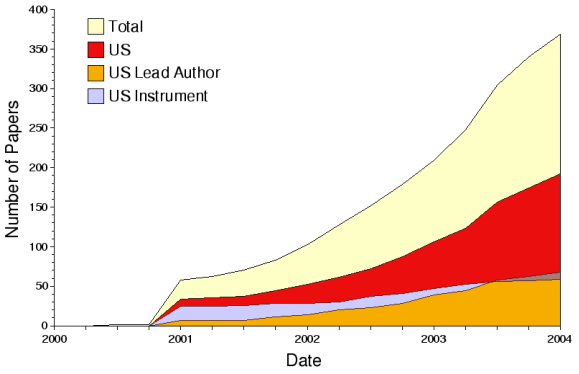

Figure 1: *XMM-Newton* publication history.

The science goals and achievements of *XMM-Newton* are directly responsive to the NASA Office of Space Science (OSS), Space Science Enterprise Strategic Plan (http://spacescience.nasa.gov/admin/pubs/strategy/2003/SpSciEntStrat(high).pdf). With respect to Table 1 of the plan, *XMM-Newton* provides unique and important data for the strategic goal of "Exploring the solar system and the universe beyond." Through our E/PO efforts and the support of university research, the project is also responsive to the goal of "Inspiring and motivating students to pursue careers in science." *XMM-Newton* allows studies of the fundamental processes of neutron stars and black holes, the creation of the elements in supernova explosions and their dispersal in supernova remnants and starburst galaxies, the evolution of the elements on the largest scale in clusters and groups of galaxies, and the distribution of dark matter in clusters, groups, and elliptical galaxies. The study of active stars allows for direct comparison with the early solar system and star forming regions for understanding the origin and evolution of stellar systems. *XMM-Newton* has determined the positions and spectral characteristics of gamma-ray bursts and examined relativistic processes from neutron stars to quasars. *XMM-Newton* also provides the unique capability of simultaneous X-ray and optical/UV observations. While there is strong potential for overlap in the science areas of *Chandra* and *XMM-Newton*, each mission has been optimized differently in the five dimensional space of angular resolution, bandpass, collecting area, spectral resolution, and timing ability. In view of the extensive proposal oversubscriptions for both programs, the world-wide astronomical community has clearly decided that both observatories are vital.

XMM-Newton observes in the 0.2–12 keV and optical-UV bands. Its large collecting area and highly elliptical orbit allow long, uninterrupted observations with unprecedented sensitivity. The contiguous coverage (up to $\sim$ 135 ks) is even more important now that *Chandra* can be limited to as little as $\sim$ 60 ks in some orientations. The observatory has three co-aligned high-throughput 7.5 m-focal-length X-ray telescopes with $6''$ full width at half maximum (FWHM) angular resolution. The European Photon Imaging Camera (EPIC) charge-coupled device (CCD) detectors provide X-ray images over a $30'$ field of view. Higher resolution spectra ($E/\Delta E \sim 200 - 800$) are provided by the Reflection Grating Spectrometers (RGS) that deflect half of the beam from two X-ray telescopes. The sixth instrument is the Optical Monitor (OM), a co-aligned 30 cm optical/UV telescope sensitive in the 1600-6500 Å band. **All the scientific instruments operate simultaneously, providing exceptionally rich data sets.** All the detectors can be run in a variety of modes, allowing them to be tuned for the science needs of a given observation.

1 XMM-Newton Science

The wealth of *XMM-Newton* results requires that we focus on a small number of what we believe are the more interesting results. We have tried to represent the broad science that *XMM-Newton* has performed but this has led us to be quite selective. Given that there have been a total of more than 1700 accepted GO proposals and almost 400 refereed papers (Figure 1), the breadth and depth of science is representative of a "Great Observatory." The following set of recent scientific results provides a taste of what has been accomplished and suggests what the future might hold.

1.1 Active Galactic Nuclei (AGN)

1.1.1 Medium-resolution Spectroscopy with EPIC

Broad Fe Kα emission lines in nearby Seyfert 1 galaxies were first observed in early *ASCA* observations, and are a key to physics near the event horizon. EPIC spectra of the bright Seyfert MCG-6-30-15 provided clues on the nature of the reprocessing medium and its physical properties. The best-fit ionized reflection model requires that the Fe Kα line is split into two reprocessing events: one from the inner disk to build up the red wing and the other from the outer accretion disk to fit the blue horn. The implied geometry is a disk that becomes strongly warped or flared at large radii (Ballantyne et al. 2003). Ponti et al. (2003) found a significant enhancement of the fractional variability in the Fe Kα energy band compared to the underlying continuum in MCG-6-30-15. This represents one of the strongest, model-independent, pieces of evidence for the presence of redshifted relativistic matter accreting into the black hole.

The high EPIC sensitivity opens up studies of classes of objects previously inaccessible to X-ray spectroscopy such as broad absorption line (BAL) quasi-stellar objects (QSOs) and low luminosity radio galaxies. *XMM-Newton* data established that the X-ray weakness of BAL QSOs is due to a large column density of a complex absorber (Grupe et al. 2003). Detailed studies of the BAL QSO Mkn 231 (Turner & Kraemer 2003) reveal strong narrow ($\sim 18,000$ km s^{-1}) neutral Fe Kα line emission similar in strength to that seen in Seyfert 1s. As opposed to Seyfert 1s, the line originates from transmission and/or reflection from a distribution of emitting clouds rather than in the accretion disk.

Relativistic outflows from the BAL quasars PG 1115+080 and APM 08279+52 (Chartas et al. 2003) with $v \sim 0.1 - 0.3$c were detected via X-ray Fe K resonance absorption. A comparison of the ionization properties and column densities of the low- and high-energy absorbers indicates that they are distinct and that there is significant variability of the energies and widths of the X-ray absorption features over timescales of 19 and 1.8 weeks

(proper time), respectively. This variability indicates that the absorbers are most likely launched at relatively small radii ($< 10^{16}$ $(M_{bh}/M_8)^{1/2}$ cm) from the black hole, a fundamental contribution to the understanding of BAL QSOs.

1.1.2 High resolution spectroscopy with the RGS

The very high signal-to-noise ratio (S/N) RGS data of MCG-6-30-15 have allowed a detailed test of the existence of relativistic emission lines from C, N, and O (Sako et al. 2003). Turner et al. (2003) show that the form of the absorption curve derived from analysis of the time variability of the RGS data does not agree with any of the existing models. After removing an empirical absorption model, the remaining residuals resemble broad emission lines from O and C, perhaps from an ionized disk. The existence of broadened Lyα emission from C, N, and O produced in the innermost regions of an accretion disk around a Kerr black hole, has also been seen in Mkn 766 by Mason et al. (2003) and NGC4051 by Ogle et al. (2004).

RGS observations have been crucial in understanding the complex link between X-rays and UV absorbers. Observation of the Seyfert 1 galaxy NGC 3783 (Figure 2, Behar et al. 2003) rejects the scenario of the warm absorber being caused by dense clumped clouds, in stark contrast to the picture of numerous clumpy clouds drawn recently from UV spectra which favor an origin in extended ionization cones ($r > 10$ pc).

EPIC and RGS observations of two QSOs (PDS 456, Reeves et al. 2003a; PG 1211+143, Pounds et al. 2003) have revealed the presence of ionized outflows with velocities from 24,000 to 50,000 km s^{-1}. These flows carry a very high mass flux and represent a significant fraction of the energy radiated in these non-BAL objects, indicating that many QSOs may be injecting very large energies into the interstellar medium (ISM) or intergalactic medium (IGM), a conclusion also reached for some lower luminosity Seyfert galaxies (Ogle et al. 2004).

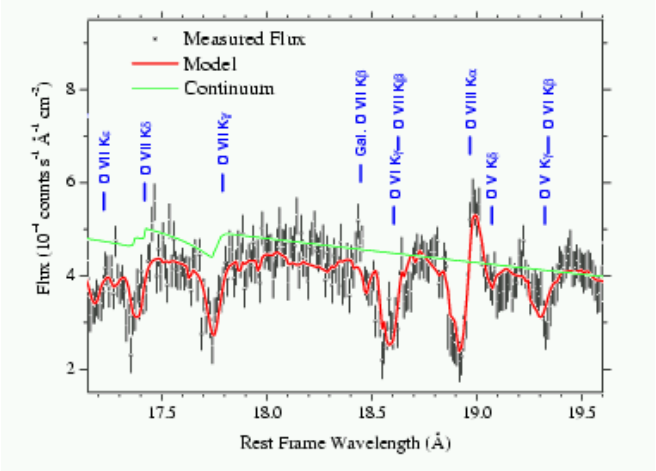

Figure 2: Spectrum of NGC 3783 showing the region of O VIII Kα as well as higher order lines (Kβ, Kγ, etc.) of lower charge states of O obtained with a 280 ks RGS observation. The thick curve represents the best-fit model and the thin curve is the continuum model with only galactic absorption (Behar et al. 2003).

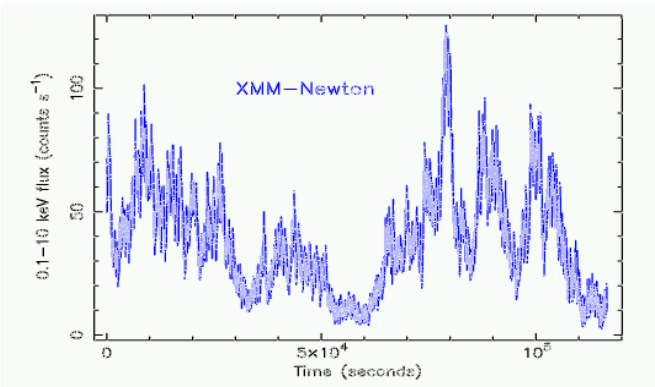

Figure 3: *XMM-Newton* lightcurve of the NLS1 NGC 4051 in the 0.1–10 keV band, with 5s time bins, combining data from the PN and MOS CCDs (McHardy et al. 2003).

1.1.3 Variability

The combination of long monitoring campaigns with *RXTE* and shorter but denser *XMM-Newton* observations has demonstrated a similarity between the power spectral densities (PSD) of Seyfert galaxies and Galactic black holes (GBH) in the "low state" (Markowitz et al. 2003), and between the PSD of the narrow line Seyfert 1 (NLS1) galaxies and the PSD of a GBH in a "high state" (Figure 3). This strengthens the case for a physical similarity between Seyfert 1 galaxies and GBH. This similarity allowed Fabian & Vaughan (2003) to estimate the AGN black masses, from which a super-Eddington emission has been inferred for Mkn 766.

Perlman et al. (2003) observed 13 X-ray bright BL Lacs and accurately determined the X-ray spectral form of this class showing power-law shapes plus curvature with no line features, either in absorption or emission. This spectral curvature must be intimately related to the process of particle acceleration in the jets producing the broad band Bl Lac spectra.

1.2 Clusters of Galaxies

XMM-Newton's high S/N imaging spectroscopy plays a key role in understanding the physics of clusters, necessary for their use as cosmological probes and for understanding the formation of large scale structure. This ability allows the measurement of the temperature and metal abundance of hot, massive clusters at $z > 1$ (Rosati et al. 2004; Hashimoto et al. 2002) which provides key empirical clues about the evolution of the cluster luminosity-temperature and mass-temperature relations over a wide range of redshifts ($z = 0.003 - 1.3$).

Clusters of galaxies are closed ecosystems, and thus provide a unique history of metal production in the universe. *XMM-Newton* has extended the knowledge of accurate metal abundances out to $z = 1.24$ (Rosati et al. 2004; Tozzi et al. 2003) showing that there is very little, if any, evolution in the Fe abundance.

RGS spectra of the central regions of low-z clusters have provided the most robust estimates of the abundances of O, Ne, and Mg, and shown significant variation in the O/Fe ratio between clusters, a result that is puzzling.

Peterson et al. (2003) analyzed 14 RGS observations of

cluster cooling flows. The absence of Fe L lines from Fe XVII-XXII strongly restricts the amount of low temperature gas from plasmas cooler than about $T_X/2 - T_X/3$, in strong contradiction to the classical cooling flow models. A coherent, physically-motivated model explaining these observations is yet to be found, yet the solution to this problem has fundamental importance for the formation of cosmic structure, since it is generally believed that all structure forms by the infall and cooling of gas in deep potential wells. Kaastra et al. (2004) fit the EPIC spectra for the same objects and found multi-temperature plasmas inside the cluster cooling radius, and a decrement of the average central temperature of the cluster, further complicating the picture. This problem also extends to lower mass systems (Mathews & Brighenti 2003), groups, and giant elliptical galaxies (Tamura et al. 2003) which also have a strong deficit of cool gas compared to the cooling flow predictions. It is unclear how one simple solution can explain these results over a factor of 1000 in object mass and a wide range of physical conditions.

Only *XMM-Newton* can measure cluster temperature gradients at radii approaching the virial radius, crucial for determining the masses of clusters. *XMM-Newton* data have shown that the temperature distribution has a self-similar shape which extends to surprisingly low temperatures and high redshifts (Pratt & Arnaud 2003), is nearly isothermal out to a large fraction of the virial radius, and has a decline with radius far from the cluster center (Zhang et al. 2004) which does not agree well with theoretical predictions. The normalization of the empirical cluster $M-T$ relation differs significantly from the theoretical one, and contrary to theoretical expectation the gas mass fraction depends on cluster mass, with higher gas mass fractions at higher total masses.

XMM-Newton data have shown that there exist a wide variety of entropies in the central regions of groups (Mushotzky et al. 2003) and that the shape of the entropy profile does not agree with standard cluster formation models. The enhanced entropy in groups is one of the few "fossils" of the formation of structure. These data indicate that there is a substantial injection of energy which radically changes our understanding of the formation of all structure.

The high S/N of *XMM-Newton* has allowed the construction of pressure and entropy maps for galaxies, groups and clusters (Figure 4, Finoguenov et al. 2004). These

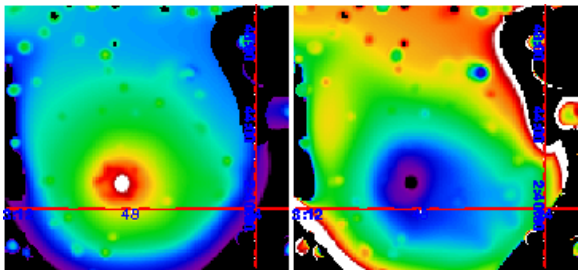

Figure 4: The pressure (left) and entropy profile (right) for the NGC4636 galaxy and group. One can directly see that the entropy and pressure maps differ, indicating the physical regions where dynamical effects are occurring.

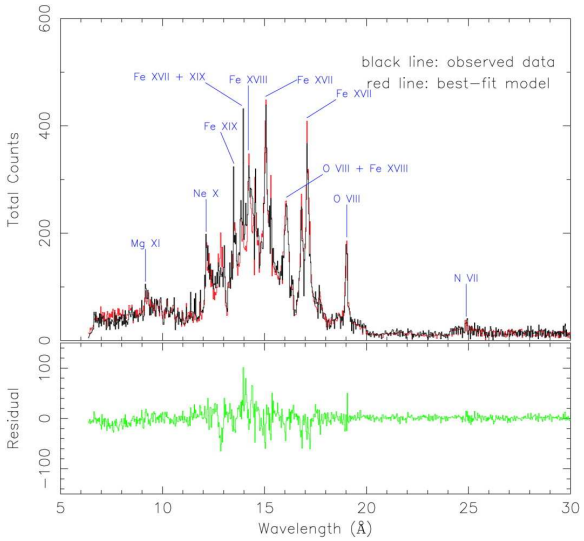

Figure 5: Co-added RGS1 and RGS2 spectrum of NGC 4636 (black line). The best-fit model, including a temperature gradient and resonance-line scattering effects, is plotted in red. The residuals to the model fit are plotted in the lower panel (Xu et. al. 2002).

maps allow the direct visualization of the distribution of energy and matter in these systems, and directly show how the deviations from the theoretical scaling relations arise.

The existence of velocity structure in the X-ray emitting gas is a natural consequence of hierarchal clustering models. *XMM-Newton* results on the Perseus cluster (Churazov et al. 2004; Gastaldello & Molendi 2004) show that the He-like Fe line in the Perseus cluster is optically thin which requires either turbulence or velocity shear to suppress resonance scattering in the central 100 kpc.

Theory predicts the existence of a warm-hot IGM which contains most of the baryons in the universe. *XMM-Newton* observations by Durret et al. (2003) and Kaastra et al. (2003) have detected the existence of soft X-ray emission from IGM filaments near both the Coma and Abell 85 clusters, as well as O VII line emission from filaments near four other clusters of galaxies. These are the first detections in emission of the main repository of baryons in the universe: the baryons in between galaxies. Future *XMM-Newton* observations have the potential for deriving the first accurate estimate of the mass in this almost invisible, but dominant, component of the universe.

1.3 Galaxies

1.3.1 Elliptical galaxies

Giant elliptical galaxies are the oldest and most massive stellar systems in the universe. *XMM-Newton* observations predominantly probe the hot X-ray emitting ISM which is the repository of the total mass loss from stellar winds, planetary nebulae, and supernovae.

The RGS spectrum of the giant elliptical galaxy NGC 4636 (Figure 5, Xu et al. 2002) provides precise abundances, and the cross-dispersion profiles of several Fe lines provide clear evidence of resonance scattering by the highest

oscillator strength lines, as well as a weak temperature gradient in the inner regions. The derived abundances cannot be reconciled with current chemical-enrichment models of elliptical galaxies and present a significant challenge for Type Ia and Type II supernova models. These results are not unique; the Fe and O abundances of NGC5044 and M87 are similar (Tamura et al. 2003). Since most stars in the universe are in galactic bulges it is clear that these results may change our fundamental understanding of the formation of stars and galaxies.

XMM-Newton observations of the elliptical galaxies NGC 3585, NGC 4494, and NGC 5322 show that the X-ray output is dominated by discrete source emission, with only little contribution from hot gas (O'Sullivan & Ponman 2003). This was interpreted as evidence that these galaxies have recently formed and have yet to build up large X-ray halos from stellar wind losses.

1.3.2 Ultra-luminous X-ray (ULX) sources

High S/N *XMM-Newton* data have allowed significant progress in understanding the nature of ULXs (possible $M \sim 100 - 1000$ M$_\odot$ black holes with source luminosities > 20 times the neutron star Eddington limit, $L_{\rm X} > 2 \times 10^{39}$ ergs s^{-1}). Miller et al. (2003) used *XMM-Newton* EPIC observations of NGC 1313 to show that the best fits were provided by a combination of soft and hard spectral components, where the soft components are represented by multicolor disk blackbody models with color temperatures of ≈ 150 eV. Assuming this soft component originates from the inner region of an accretion disk, black holes with intermediate masses ($M_{\rm BH} \approx 10^3\ M_\odot$) are inferred.

The *XMM-Newton* EPIC discovery of quasi-periodic oscillations (QPOs) in an M82 ULX has provided compelling evidence for the presence of a geometrically thin accretion flow, and (along with the observed broad Fe-K line) argues that the emission is not strongly beamed, giving strong weight to a very high mass for this object (Strohmayer & Mushotzky 2003). The detection of a "Cyg X-1 like" power density spectrum for one of the ULXs in NGC4559 with a break at ~ 30 mHz also indicates a high mass of $M \sim 500_\odot$ (Cropper et al. 2004). Only *XMM-Newton* has the S/N to determine these characteristic properties of high mass black holes in nearby galaxies.

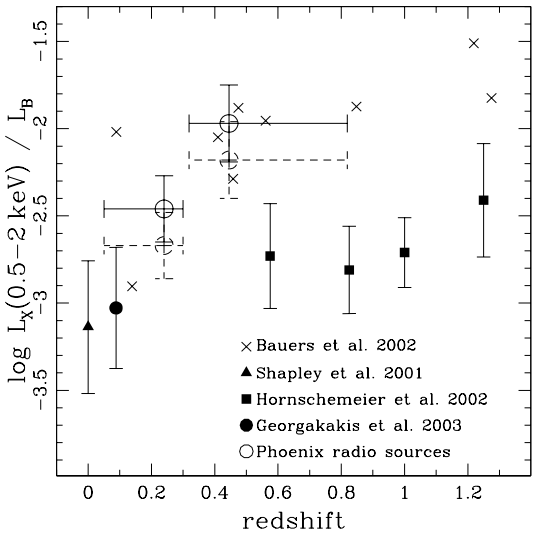

Figure 6: Ratio of soft-band X-ray to B-band luminosity against redshift for normal spiral galaxies (filled symbols) and late-type radio sources (open symbols). Circles are from the *XMM-Newton*/2dF and Phoenix Deep Survey (Georgakakis et al. 2003b).

1.3.3 Evolution of Galaxies

A statistical sample of 235 normal galaxies from the *XMM-Newton*/2dF survey covering ≈ 1.5 deg^2 was used to study the evolution of spiral and elliptical galaxies at redshifts $z \approx 0.1$ (Georgakakis et al. 2003a). In combination with a stacking analysis of normal galaxies from the *Chandra* Deep Fields at $z = 0.4$–1, the data allowed, for the first time, measurement of the X-ray properties and evolution of galaxies over cosmologically interesting distances. The combined analysis suggests little or no evolution of the X-ray production mechanism compared to the optical, with $L_{\rm X}/L_B$ values consistent with those of both local (< 100 Mpc) and distant ($z \approx 1$) samples of galaxies (Figure 6).

1.4 Supernova Remnants and Neutron Stars

As extended objects with high temperatures and a complex set of abundances and ionization conditions, supernova remnants (SNRs) are prime objects for study with *XMM-Newton*. Spatially resolved SNR spectra can identify stratification of ejecta, separate the forward and reverse shock regions, measure spatial variations in temperature and ionization conditions, and search for the compact hard emission of a pulsar or nebula. The large effective area and good angular resolution of *XMM-Newton* provide rich spectra on physically important spatial scales. In addition, the RGS features a large dispersion angle which suppresses the spatial-spectral confusion. *XMM-Newton* provides the capabilities for high resolution spectroscopy of SNRs with radii up to several arc minutes uniquely permitting the use of line diagnostics for density and ionization-state determinations, as well as velocity measurement.

The relative abundances and distribution of the ejecta in SNRs provide information on the mass for the progenitor star as well as on the detailed physical processes by which heavy elements are distributed into the ISM. In

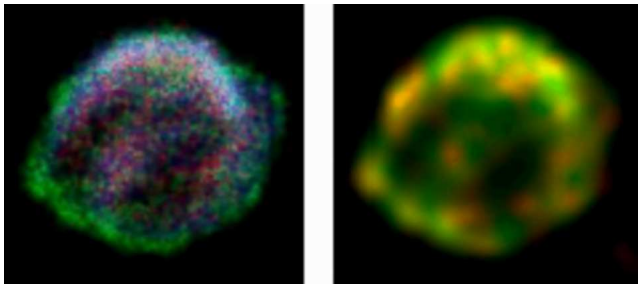

Figure 7: Left: EPIC pn three color image of the Kepler SNR in Si (blue), Fe K (red), and 4-6 keV high energy continuum (green). Right: MOS+pn two color image of the high energy continuum (green: 4–6 keV, red: 8–10 keV; Cassam-Chenai et al. 2003).

particular, various degrees of mixing are evident based on the spatial distribution of equivalent width maps, and on Doppler mapping of particular ion species. In Kepler's SNR, for example, EPIC radial profiles show that the Si-K emission extends to a larger radius than the Fe-L emission, particularly in the southern part of the remnant (Figure 7, Cassam-Chenai et al. 2004). This is in striking contrast to the structure in Cas A where a distinct inversion of the Si- and Fe-rich ejecta layers is observed. The Fe-K emission in Kepler is observed to peak at a smaller radius then Fe-L, indicating that the temperature increases inwards in the ejecta component.

1.4.1 SNR Dynamics: Ejecta Emission and Shocks

Several thousand supernovae (SNe) have been identified in the optical to date, whereas only ∼30 SNe have been detected in the radio and 20 in the X-ray band. The discovery of the Type Ic SN 2002ap with the OM and EPIC instruments five days after its outburst represents an important case since it is one of only three Type Ic SNe detected in X-rays. In contrast to other X-ray emitting SNe, SN 2002ap was not dominated by hard X-ray emission at early times, and had a faster rate of decline. The observed prompt soft X-ray emission (0.8 keV) was interpreted to originate from the interaction of the reverse shock with a low-density ($\dot{M} \approx 5 \times 10^{-7}$ $M_\odot$ yr^{-1}) and fast ($v_w \approx$ (1–3) $\times 10^4$ km s^{-1}) stellar wind. Unlike other Ic events such as SN 1998bw, there was no evidence for relativistic ejecta or beaming, and the low inferred total energy (5×10^{51} ergs s^{-1}) argues against a classification as a hypernova (Soria et al. 2004).

Deep observations of Cas A with *XMM-Newton* permit detailed spectral fitting on scales of $20'' \times 20''$, and show that the spatial distributions of Si, S, Ar, and Ca are highly correlated (Willingale et al. 2002). The inferred abundances are consistent with predicted nucleosynthesis yields from a progenitor whose mass was $\sim 12 M_\odot$ at the time of explosion. The abundance ratios for Ne, Mg, and Fe are much different than the ratio of S, Ar, and Ca (all relative to Si), as expected from current nucleosynthesis models. The EPIC spectra allow a determination of Doppler velocities along line of sight. Combined with radial position information, this provides a measurement of the SNR dynamics. These measurements show that the Si-K and S-K emission from the cool plasma component originates in a narrow ejecta shell while the hotter Fe-K emission is expanding somewhat more rapidly and is concentrated primarily in two large clumps that appear to originate from ablation of ejecta bullets.

1.4.2 Pulsars and Pulsar Wind Nebulae

X-ray emission from pulsars can have several origins: magnetospheric processes, polar caps that have been heated by instreaming particles, or the entire neutron star (NS) surface due to cooling of the interior. Observations of PSR B0656+14 reveal all three of the above components, with a pulse shape and pulsed fraction that is highly dependent upon energy, while PSR J0633+1746 shows evidence of surface cooling and a power law component (Zavlin & Pavlov 2003). In both cases, the thermal component requires an emission size that is smaller than expected when modeled as a blackbody, while current atmosphere models require areas that are too large. For the Vela pulsar, RGS observations (Mori et al. 2003) reveal a featureless spectrum, ruling out a heavy element atmosphere and suggesting the presence of hydrogen. The inferred temperature of $T^\infty \sim (6.4 - 7.1) \times 10^5$ K falls well below standard cooling curves for a neutron star of its age ($\sim 10^4$ yr), providing significant constraints on the interior structure.

The high throughput provided by *XMM-Newton* is crucial in identifying faint pulsar wind nebulae (PWN) which are a signature of young neutron stars. Recent observations of the composite SNR G16.7+0.1 reveal the PWN, making this one of the faintest such systems detected in X-rays (Helfand et al. 2003). An *XMM-Newton* survey of portions of the Galactic Plane has detected the composite SNR G20.0−0.2 for the first time in X-rays, and revealed over 400 sources including a number of known SNRs and HII regions (Hands et al. 2004).

In the composite SNR CTA 1, *XMM-Newton* observations confirm that the compact source RX J0007.0+7302 located at the center is the neutron star powering the system (Slane et al. 2004). No pulsations are detected and the spectrum is a power law with an additional soft thermal component that may correspond to emission from hot polar cap regions or to cooling emission from a light-element atmosphere over the entire star. The power law spectrum is consistent with that extrapolated from the gamma-ray source 3EG J0010+7309, supporting the suggestion that there is a gamma-ray emitting pulsar at the center of CTA 1.

1.5 GRBs, XRBs, and CVs

1.5.1 Gamma-ray Bursts (GRBs)

The large collecting area and fast response time of *XMM-Newton* has allowed the measurement of the X-ray spectra of GRBs at early times when they are bright, as well as their evolution over the duration of the observation. Willingale et al. (2004) show that the evolution of the X-ray spectral index follows closely the evolution of the optical spectral index, a strong prediction of the standard GRB model, and that there is no deviation from the best-fit afterglow model seen in the X-ray decline indicating that the excess optical and radio flux from 1–5 days arises from a later injection of slower electrons by the central engine. *XMM-Newton* observations of GRB 031203 have revealed a ring around the GRB caused by scattering of soft X-rays from foreground dust in the Milky Way (Vaughan et al. 2004, see Figure 8). The evolution of the brightness and size of the ring provide strong evidence for a prompt, soft X-ray flash from the GRB. *XMM-Newton* observations of GRB 980425 two years after the event have detected emission from the associated supernova 1998bw, bolstering GRB-supernova association. *XMM-Newton* data have also provided the best evidence to date of X-ray emission lines in the spectra of the GRB afterglow (Reeves et al. 2003b).

1.5.2 X-Ray Binaries in the Milky Way

XMM-Newton has obtained detailed spectroscopic data of virtually all the bright sources revealing the highly complex conditions of the X-ray emitting plasma. Its sensitivity has allowed the measurement of spectra of

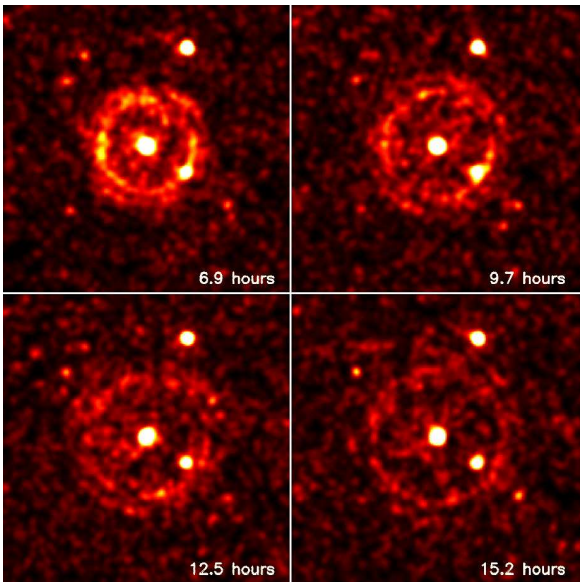

Figure 8: EPIC images of the expanding ring of the gamma-ray burst GRB 031203. The slowly fading afterglow of the GRB is at the center of the expanding ring (Vaughan et al 2004).

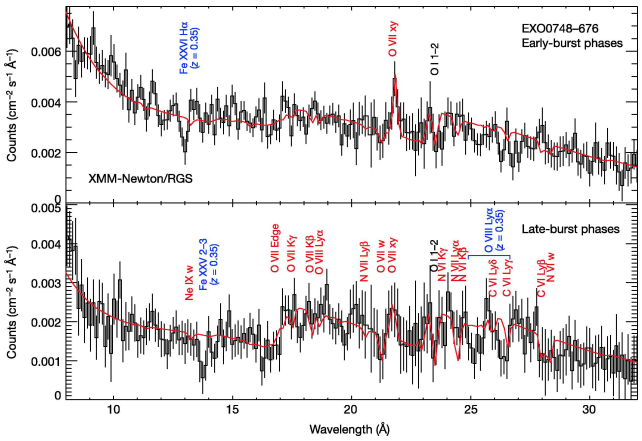

Figure 9: Summed RGS spectra of the low mass X-ray binary EXO0748-676 (Cottam et al. 2002). These spectra highlight the observed radiative recombination complexes (RRC) of O VII and N VII, and C VI Lyα at 0.35.

many transient sources in their quiescent states, and detailed spectra of low-luminosity X-ray sources in globular clusters, neither of which are possible with any other instrument.

One of the most exciting *XMM-Newton* results has been the detection of line features closely associated with the surface of the neutron star EXO0748-676 at a redshift of 0.35 (Figure 9, Cottam et al. 2002). This has for the first time constrained the mass-radius relation via the gravitational redshift of spectral lines produced in the neutron star photosphere. This relation is completely consistent with models of neutron stars composed of normal nuclear matter, while it excludes some models in which the neutron stars are made of more exotic matter.

1.5.3 X-Ray Binaries in Other Galaxies

XMM-Newton affords us the ability to study extragalactic populations of X-ray binaries in detail, which is a qualitative advance over what is possible with other instruments. In particular, because of its large collecting area, *XMM-Newton* can obtain spectra of individual sources as well as light-curves with high S/N ratio. The combination of spectral and timing properties makes it possible to ascertain the nature of many of the sources based on the *XMM-Newton* data alone. So far, *XMM-Newton* has surveyed many of the galaxies in the local group (e.g., M31, M33, the Magellanic Clouds) and has revealed the properties of their source populations down to very faint levels. It has also surveyed more distant galaxies (such as M101). For example, the limiting luminosity reached in M31 is a few times 10^{34} erg s^{-1} (Trudolyubov et al. 2002a); these deep observations have shown systematic differences between the source populations in the disk and bulge of M31, and revealed the complexities of their luminosity functions. An excellent example of detailed source studies is provided by the deep survey of M31 which has resulted in the detection of a black hole candidate (Barnard et al. 2003) and the discovery of periodic intensity dips at a period of 2.78 h in the X-ray source in the globular cluster Bo 158 in M31 (Trudolyubov et al. 2002b).

1.5.4 Cataclysmic Variables (CVs)

Most (CVs) are low flux and low luminosity X-ray sources, $L_X \sim 10^{31}$–10^{33} erg s^{-1}, limiting previous missions to small samples. *XMM-Newton* can obtain phase-resolved spectroscopy of many CVs, and the combination of the simultaneous UV photometry from the OM is unique. An *XMM-Newton* snapshot survey of 37 polars (Ramsay et al. 2004) showed that 16 of these systems were in a low, or much reduced, accretion state. Of those, 6 were not detected in X-rays. Of the 10 systems which were detected at low but significant rates in X-rays, 8 showed significant variability in their X-ray light curves. This implies that non-uniform accretion still takes place during low accretion epochs. The bolometric luminosity of these systems is $\sim 10^{30}$ ergs s^{-1}, two orders of magnitude less than systems in a high accretion state. The X-ray and simultaneous OM UV data imply that a low temperature component exists but its temperature is outside the bandpass of X-ray instruments.

1.6 Stars and Planets

XMM-Newton's properties make it an excellent facility to observe X-ray emission from stars, which is dominated by thermal processes and usually peaks in the *XMM-Newton* energy band. The results highlighted below just scratch the surface of how *XMM-Newton* is advancing our understanding of stellar X-ray emission and leading to new results concerning the birth, growth and death of stars.

1.6.1 Measuring Stellar Coronae

XMM-Newton has been used to measure the geometries, densities, abundances and activity of a large sample of stellar coronae. Sanz-Forcada et al. (2004) put together three years worth of *XMM-Newton* and *Chandra* observations of the ultra-rapid rotator AB Dor, showing that

the emission measure distribution does not change with the changing flux, and that higher temperature gas is under higher pressure – inconsistent with constant pressure loop models. Marino et al. (2004) find evidence for rotational modulated X-ray emission in the supersaturated star VXR45a in IC 2391, suggesting that a significant part of the coronal emission arises in the equatorial region close to the star. Kastner & Soker (2003) used *XMM-Newton* observations of highly evolved AGB stars to determine the importance of magnetic fields in channeling mass loss and shaping planetary nebula. They detected emission from Mira, possibly due to accretion or magnetic activity associated with its companion.

1.6.2 Massive Single Stars & Colliding Wind Binaries

X-ray emission from massive single stars is believed to be dominated by shocked gas distributed throughout a radiatively-driven, dense, unstable stellar wind. The distribution of these shocks and their influence on the stellar wind itself has not yet been resolved observationally despite more than 20 years of study. *XMM-Newton*, by obtaining simultaneous high S/N X-ray light curves and spectra, measures the real emission measure distribution, the amount of wind absorption, and the hydrodynamics of the shocked gas. RGS spectra (Mewe et al. 2003) measured the abundances and the spatial distribution of the wind shocks in τ Sco. The ratio of the He-like forbidden to intercombination lines suggests that cooler X-ray emitting gas (2–8$\times10^6$ K) arises close to the star, while hotter emission (20–40$\times10^6$ K) is produced by slow dense blobs embedded throughout the fast ambient stellar wind. The ratios of the He-like line components in RGS spectra strongly constrain the location of the hotter emitting gas, while upper limits on the location of the plasma derived from lower energy lines show that they originate from a few dozen to hundreds of stellar radii (Paerels & Kahn 2003).

The superluminous, unstable star Eta Carinae is one of the most massive in the Galaxy and undergoes an X-ray eclipse/"shell event" every 5.5 years. *XMM-Newton*'s monitoring of Eta Car's X-ray spectrum (Hamaguchi et al. 2003) showed that the X-ray eclipse is partial, and that during the eclipse minimum the source flux increases in a surprisingly simple way, the absorption is higher than normal, and the temperature distribution stays fairly constant. The observations are qualitatively in agreement with the "colliding wind binary model " and they suggest that Eta Car is orbited by an otherwise hidden companion. Leutenegger et al. (2003) published RGS spectra of the X-ray emitting shocked gas which was ejected by Eta Car a few centuries ago, and which now surrounds the star. These spectra show strong emission from H and He-like lines of N, Ne, Fe and Mg, and a high N/O ratio of > 9, implying that this material was produced by CNO processing. This N/O ratio is difficult to reconcile with previous estimates of the He abundance unless the star was rotating rapidly at the time of the ejection event.

1.6.3 Star Formation

XMM-Newton's wide field of view and sensitivity are well suited to the study of star formation regions and identification of faint sources like intermediate mass young stars, embedded sources and brown dwarfs. In the star formation region L1551, Favata et al. (2003) detected most of the known pre-main sequence stars and found a dichotomy in elemental abundance between the weak-lined and classical T-Tauri stars, despite similar photospheric abundances. They also detected significant column density variations in the source XZ Tau, suggesting that some or all of the X-ray emission is due to accretion processes. In the Serpens dark cloud, Preibisch (2003) detected 45 individual sources but none of the Class 0 protostars and only 1 of the Class I stars. However, in the massive star forming region IRAS 19410+2336, Beuther et al. (2003) detected X-ray emission from embedded intermediate-mass protostars, possibly due to magnetic interactions between the stars and their stellar disks.

1.6.4 Planets

Ness et al. (2004) detected X-ray emission from Saturn. In contrast to the X-ray emission from Jupiter which is dominated by the aurora, the emission from Saturn is consistent with elastic and fluorescent scattering of solar X-rays, albeit with the requirement of a rather high albedo. The emission intensity of Saturn is similar to that of Jupiter in its equatorial region.

1.7 Diffuse Emission

The diffuse X-ray background is the sum of emission from several different regions of hot plasma from the local ISM and Galactic halo to the Local Group and intercluster medium (ICM), including stellar-wind bubbles, old SNRs, and superbubbles. Studies of these sources require large effective areas to provide sufficient counts, large solid angles, good angular resolution for the removal of contaminating point sources, low detector background for high S/N, and spectral response down to ~ 0.2 keV, covering the energies where the Galactic halo and the hot IGM are most easily observed. X-ray emission often provides the only mechanism for the observation of these sources, a major component of the galactic and intergalactic environment.

1.7.1 Hot Gas in the S308 Circumstellar Bubble

Fast stellar winds from massive stars can sweep up the ambient medium to form bubbles. The bubble interiors should be filled with the hot shocked fast winds, ejected by the red supergiant progenitor of the central Wolf-Rayet (WR) star. However, S308 is one of only two single-star bubbles that show detectable diffuse X-ray emission. *XMM-Newton* observations of the northwest quadrant of S308 reveal the distribution of diffuse X-ray emission, which is confined within the optical shell. (See the cover page figure: the *XMM-Newton* EPIC image of the northwest quadrant of the WR bubble S308. Right: A color composite of the X-ray (blue), [O III] λ5007 (green), and Hα (red) images of the same region, Chu et al. 2003.) Spectral analysis of the diffuse X-rays show plasma temperatures of $\sim 1 \times 10^6$ K and a N/C ratio that is 15-20 times the solar value. The mass of the hot gas exceeds that of the fast stellar wind, indicating that mixing of cool gas from the dense swept-up shell into the hot interior must have occurred.

1.7.2 Nonthermal X-ray Emission from N51D

XMM-Newton observations of the superbubble N51D in the Large Magellanic Cloud (LMC) show both line features below 1.5 keV and featureless continuum from 1.5 to 3 keV, which can be fitted only if a power-law component, in addition to a thermal plasma component, is included. The presence of nonthermal X-ray emission is puzzling. The total thermal energy in the hot gas and kinetic energies in the interstellar gas are a factor of 3 lower than the total stellar energy, i.e., the mechanical energies of the fast stellar wind and supernova explosions expected from the actual stellar content (Cooper et al. 2004).

1.7.3 The North Polar Spur (NPS)

In a detailed spectral analysis of the emission from the NPS, the limb-brightened edge of a nearby superbubble, Willingale et al. (2003) show that three distinct components are required to fit the spectrum: a $T \sim 0.1$ K unabsorbed component from the local ISM, an absorbed component at roughly the same temperature which likely lies in the Milky Way halo, and a hotter component ($T \sim 0.26$ keV) representing emission from the North Polar Spur itself. The high-quality spectrum of the NPS allowed the temperature and abundances of the emission to be measured with unprecedented accuracy, and the detection of depletions in O and Ne, as well as Mg and Fe to a lesser extent. This is the first detailed abundance measurement of the hot phase of the ISM.

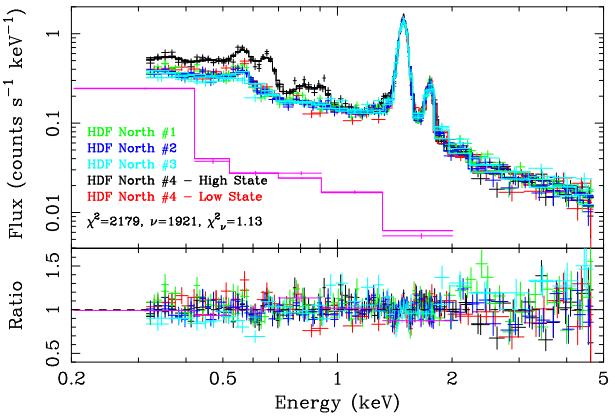

Figure 10: Fitted MOS and *ROSAT* All-Sky Survey spectra (RASS) for the four observations of the *Hubble* Deep Field North. The black curve and data are from the last of four observations of the field (2001 June 1–2) showing SWCX emission. The red, green, blue, and light blue curves and data are from the three other observations, and the low count-rate period of the fourth. The lower data (purple) are from the RASS (scaled by a factor of 100 for display purposes).

1.7.4 Solar Wind Charge Exchange (SWCX) Emission

X-ray emission produced by charge exchange between the solar wind and diffuse material within the solar system was first observed from comets. Recently, SWCX emission was serendipitously discovered in an *XMM-Newton* observation of the *Hubble* Deep Field North (Snowden et al. 2004). It is not yet clear whether the emission (Figure 10) is from interstellar neutrals within the heliosphere or from exospheric material since the emission is sampling the integral of material along the line of sight. The SWCX emission is comprised of very strong O VII, O VIII, Ne IX, and Mg XI, as well as lines from C and N.

1.8 Cosmology, Surveys, and Serendipitous Science

Surveys with *XMM-Newton* are complementary to *Chandra* data. While *XMM-Newton* reaches fluxes of 10^{-14} ergs cm^{-2} s^{-1} faster than *Chandra*, has a wider field of view, and can obtain spectra and time-variability data more readily, *Chandra* provides the precision positions necessary for optical follow-up work (Page et al. 2003). These surveys have radically altered our view of the evolution, total number, and site of AGN activity in the universe, showing that optically selected AGN produce only $\sim 20\%$ of all the energy ever radiated by massive black holes (Marconi et al. 2003).

XMM-Newton deep surveys have shown that the number counts around fluxes of 10^{-14} ergs cm^{-2} s^{-1} (the flux decade of peak contribution to the X-ray background) are dominated by AGN with $L_X \sim 10^{44}$ ergs s^{-1}, with less than half of them showing evidence of AGN activity in their optical spectra (Miyaji et al. 2004), and that the accretion luminosity of the universe peaks at a redshift of ~ 1. In the Groth-Westphal *Hubble* deep survey region, the majority of *XMM-Newton* sources with redshift information have bulge components which are resolved in *Hubble* data. These AGN are estimated to have X-ray luminosities ranging from 0.3% – 10% of the Eddington luminosity, implying that the massive black holes have either previously gone through a phase of much greater accretion or else their lifetimes as AGN are extremely long ($> 10^9$ y).

One third to one half of the *XMM-Newton* survey sources are narrow-line objects or absorption-line galaxies, with lower X-ray luminosities than the broad-lined objects. *XMM-Newton* spectra show that half of these narrow-lined objects are intrinsically absorbed AGN, but there is also a population of unabsorbed AGN without broad optical emission lines.

The wide field of *XMM-Newton* has allowed the collection of X-ray spectra for a large number of sources in the flux range from 5×10^{-14} to 3×10^{-13} ergs cm^{-2} s^{-1}, a range not previously accessible. The *XMM-Newton* spectra of these objects (Mainieri et al. 2002; Piconcelli et al. 2003) have shown that, contrary to all the models developed to explain the X-ray background spectrum, only 30% of the sources responsible for $> 25\%$ of the X-ray background show evidence for absorption in the line of sight. This result, combined with the very different distribution in redshift of the *XMM-Newton* sources from the unified background models, has been a basis for a radical revision in our understanding of the evolution of AGN (Fiore et al. 2003; Ueda et al. 2003). The extremely deep Lockman Hole observations (Hasinger 2003) have 330 sources with more than 200 counts and 104 have > 1000 counts, allowing detailed studies of the time variability and properties of the sources of the X-ray background. Many of these (Fiore et al. 2003) have

very high X-ray to optical ratios, similar to the sources that make up the X-ray background but their relative brightness has allowed detailed studies which show that they do not have broad optical lines and thus are the high luminosity analogs of Seyfert 2s, objects that were thought to be very rare.

1.8.1 SSC X-ray Source Catalog

The first Science Survey Consortium (SSC) catalog of *XMM-Newton* X-ray sources was released 2003 April. It contains detections drawn from 585 *XMM-Newton* EPIC observations made between 2000 March and 2002 May. There are 33,026 confirmed X-ray point sources with a further 23,685 detections of lower likelihood. The median flux (in the 0.2–12 keV energy band) is $\sim 3 \times 10^{-14}$ ergs cm^{-2} s^{-1}; $\sim 12\%$ have fluxes below 1×10^{-14} ergs cm^{-2} s^{-1}. The catalog contains broad band X-ray flux ratios, thumbnail X-ray images, an extensive set of links to optical, IR, and radio catalogs, and optical images via SIMBAD for many of the sources. This is the largest database of X-ray sources since the *ROSAT* all sky survey, but represents only 10% of what will eventually be available.

This catalog will be updated and enhanced in the next year with the new Science Analysis System (SAS) Version 6 reprocessing products and considerably more observation data sets, and should contain $\sim 130,000$ detections as well as light curves and X-ray spectra for many of the objects. In parallel with the catalog effort there is a major program of optical imaging of selected X-ray source fields – the XID Imaging program. As of last fall there was multi-color optical imaging to $r' \sim 24$ for ~ 200 fields, and since $> 70\%$ of *XMM-Newton* sources have a counterpart at this optical sensitivity we expect identifications for $> 10^4$ *XMM-Newton* sources! At present ~ 80 fields are public, and include extensive documentation.

References

Ballantyne, D. R. et al. 2003, MNRAS, 342, 239
Barnard, R. et al. 2003, A&A, 405, 505
Behar, E. et al. 2003, ApJ, 598, 232
Beuther, H. et al. 2003, A&A, 395, 169
Chartas et al. 2003 ApJ, 595, 85
Chu, Y.-H. et al. 2003, ApJ, 599, 1189
Churazov, E. et al. 2004, MNRAS, 347, 29
Cooper, R. L. et al. 2004, astro-ph/0401431
Cottam, J. et al. 2002, Nature, 420, 51
Cropper et al. 2004, astro-ph/0311302
Davis, D. S., & Mushotzky, R. F. 2003, astro-ph/0312211
Durret, F. et al. 2003, A&A, 403, L29
Fabian, A. C. & Vaughan, S. 2003, MNRAS, 340, 28
Favata, F. et al. 2003, A&A, 403, 187
Fiore, F. et al. 2003, A&A, 409, 79
Gaensler, B. M. et al. 2003, ApJ, 588, 441
Gastaldello, F. & Molendi, S. 2004, ApJ, 600, 670.
Georgakakis, A. et al. 2003a, MNRAS, 344, 161
Georgakakis, A. et al. 2003b, MNRAS, 345, 939
Grupe, D. et al. 2003, AJ, 127, 1159
Hamaguchi, K. et al. 2003, AAS, 203, 58.02
Hands, A. et al. 2004, MNRAS, in press
Hashimoto, Y. et al. 2002, A&A, 381, 841
Hasinger, G. 2003, astro-ph/0310804
Helfand, D. J. et al. 2003, ApJ, 592, 941
Kaastra, J. S. et al. 2003, A&A, 397, 445
Kaastra, J. S. et al. 2004, A&A, 413, 415
Kastner, J. H. & Soker, N. 2003, BAAS, 203, 3101
Leutenegger, M. A. et al. 2003, ApJ, 585, 1015
Mainieri, V. et al. 2002, A&A, 393, 425
Marconi, A. et al. 2003, astro-ph/0311619
Marino, A. et al. 2004, A&AL, in press
Markowitz, A. et al. 2003, ApJ, 593, 96
Mason, K. O. et al. 2003, ApJ, 582, 95
Mathews, W. & Brighenti, F. 2003, ARA&A, 41, 191
McHardy, I. M. et al. 2003, astro-ph/0311220
Mewe, R. et al. 2003, A&A, 398, 203
Miller, J. et al. 2003, ApJ, 585, L37
Miyaji, T. et al. 2004, astro-ph 0402617
Mori, K. et al. 2003, astro-ph/0306517
Mushotzky, R. F. et al. 2003, astro-ph/0302267
Ness, J.-U. et al. 2004, A&A, 414, L49
Ogle, P. M. et al. 2004, astro-ph/0401173
O'Sullivan, E., & Ponman, T. J. 2003, astro-ph/0312266
Paerels, F. & Kahn, S. 2003, ARAA, 41, 291
Page, K. L. et al. 2003, AN, 324, 101
Perlman, E. S. et al. 2003, BAAS, 203, 146.05
Peterson, J. R. et al. 2003, ApJ, 590, 207
Piconcelli, E. et al. 2003, A&A, 412, 6
Ponti, G. et al. 2003, astro-ph/0312250
Pounds, K. A. et al. 2003, MNRAS, 345, 705
Pratt, G. W. & Arnaud, M. 2003, A&A, 408, 1
Preibisch, T. 2003, A&A, 410, 951
Ramsay, G. et al. 2004, astro-ph/0402526
Reeves, J. N. et al. 2003a, ApJ, 593, L65
Reeves, J, N. et al. 2003b, A&A, 403, 463
Rosati, P., et al. 2004, AJ, 127, 230
Sako, M. et al. 2003, ApJ, 596, 114
Sanz-Forcada, J. et al. 2004, A&A, in press
Slane, P. et al. 2004, ApJ, 601, 1045
Snowden, S. L. et al. 2004, ApJ, submitted
Soria, R. et al. 2004, A&A, 413, 107
Strohmayer, T., & Mushotzky, R. 2003, ApJ, 586, L61
Tamura, T. et al. 2003, A&A, 399, 497
Tozzi, P. et al. 2003, ApJ, 593, 705
Trudolyubov, S. P. et al. 2002a, ApJ, 571, L17
Trudolyubov, S. P. et al. 2002b, ApJ, 581, L27
Turner, A. K. et al. 2003, MNRAS, 346, 833
Turner, T. J. & Kraemer, S. B. 2003, ApJ, 598, 916
Ueda, Y. et al. 2003, ApJ, 598, 886
Vaughan, S. et al. 2004, astro-ph/0312603
Willingale, R. et al. 2002, A&A, 381, 1039
Willingale, R. et al. 2003, MNRAS, 343, 995
Willingale, R. et al. 2004, astro-ph/0307561
Xu, H. et al. 2002, ApJ, 579, 600
Zavlin, V. E. & Pavlov, G. G. 2003, astro-ph/0312326
Zhang, Y.-Y. et al. 2004, A&A, 413, 49

Appendix 2: List of Acronyms

2dF	Two Degree Galaxy and Quasar Survey
AAVSO	American Association of Variable Star Observers
AAS	American Astronomical Society
ADP	Astrophysics Data Program
AGN	Active Galactic Nuclei
AO	Announcement of Opportunity
ASCA	Advanced Satellite for Cosmology and Astrophysics
BAL	Broad Absorption Line
CCD	Charge-Coupled Device
CCF	Current Calibration Files
CLEA	Contemporary Laboratory Experiences in Astronomy
CMU	Carnegie Mellon University
Co-I	Co-Investigator
CTI	Charge Transfer Inefficiency
CU	Columbia University
CV	Cataclysmic Variable
DPU	Digital Processing Unit
EA	Educator Ambassadors
EPIC	European Photon Imaging Camera
E/PO	Education and Public Outreach
ESA	European Space Agency
FTE	Full Time Equivalent
FWHM	Full Width at Half Maximum
FY	Fiscal Year
GALEX	Galaxy Evolution Explorer
GBH	Galactic Black Hole
GLAST	Gamma-ray Large Area Space Telescope
GO	Guest Observer
GOF	NASA/GSFC Guest Observer Facility
GRB	Gamma-Ray Burst
GSFC	Goddard Space Flight Center
GT	Guaranteed Time
GTN	Global Telescope Network
HEASARC	High Energy Astrophysics Science Archive Research Center
HETG	High Energy Transmission Grating
HPD	Half Power Diameter
ICM	Intercluster Medium
IGM	Intergalactic Medium
INTEGRAL	International Gamma-Ray Astrophysics Laboratory
IR	Infra Red
IRAS	Infra Red Astronomical Satellite
ISM	Interstellar Medium
ITEA	International Technology Education Association
JPL	Jet Propulsion Laboratory
LANL	Los Alamos National Laboratory
LETG	Low Energy Transmission Grating
LMC	Large Magellanic Cloud
LTI	Learning Technologies, Inc.
LTSA	Long Term Support in Astrophysics
MOS	MOS style EPIC CCD detector
MSSL	Mullard Space Science Laboratory
NASA	National Aeronautics and Space Administration
NLS1	Narrow Line Seyfert 1
NPS	North Polar Spur
NS	Neutron Star
NSF	National Science Foundation
NVO	National Virtual Observatory

OM	Optical Monitor
OSS	Office of Space Science
PGP	Pretty Good Privacy
PI	Principal Investigator
PIMMS	Portable, Interactive Multi-Mission Simulator
PN	PN style EPIC CCD detector
PSD	Power Spectral Density
PSF	Point Spread Function
PWN	Pulsar Wind Nebula
QPO	Quasi-Periodic Oscillation
QSO	Quasi-Stellar Object
RASS	*ROSAT* All-Sky Survey
RGS	Reflection Grating Spectrometer
RMS	Root Mean Square
ROSAT	Röntgen Satellite
RPS	Remote Proposal System
RRC	Radiative Recombination Complexes
RTRD	Real Time Raw Data
RXTE	Rossi X-ray Time Explorer
SAS	Science Analysis System
SEU	Structure and Evolution of the Universe
SN	Supernova
S/N	Signal to Noise
SNR	Supernova Remnant
SOC	Science Operations Center
SSC	Survey Science Centre
SSU	Sonoma State University
SWCX	Solar Wind Charge Exchange
TOO	Target of Opportunity
UC	University of California
UCB	University of California, Berkeley
UCR	University of California, Riverside
UCSB	University of California, Santa Barbara
UV	Ultra Violet
WR	Wolf-Rayet
UK	United Kingdom
ULX	Ultra-Luminous X-ray source
US	United States
XID	X-ray source IDenfication program
XMM-Newton	Newton X-ray Multi-Mirror
XRB	X-ray Binary
XSA	*XMM-Newton* Science Archive